Appl. Phys. B 73, 119–123 (2001) / Digital Object Identifier (DOI) 10.1007/s003400100627

**Applied Physics B**
Lasers
and Optics

# Generation of high-quality 10-femtosecond laser pulses with intracavity spatial and spectral control

**J.Y. Zhou***, **C.J. Zhu, J. Kuhl**

Max-Planck-Institut für Festkörperforschung, Heisenbergstr. 1, 70569 Stuttgart, Germany

Received: 11 June 2001/Published online: 18 July 2001 – 

**Abstract.** Spatial and spectral control, using an intracavity capillary and a slit, is applied to improve the output pulse quality of a Ti:sapphire laser. Satellite-free 10-fs optical pulses with a smooth spectral and spatial profile have been generated. Employing a root-mean-square formalism for pulse characterization, spatial, spectral and temporal intensity distributions are analyzed for laser pulses with a duration as short as three to four optical cycles.

**PACS:** 42.60.Jf; 42.65.Re; 42.65.Tg

Sub-10-fs optical pulses with a spectral bandwidth of more than 100 nm can now be directly generated from solid-state laser oscillators [1–3]. However, these laser pulses very often show pronounced structures in the frequency, time and spatial domain [4–8]. For many practical applications of sub-10-fs optical pulses, the presence of such spatial, temporal and spectral sub-structures strongly influences the experimental results. Obviously, the characterization of an optical pulse using the full width at half-maximum (FWHM) of autocorrelation curves does not correctly take into account the pulse distortion related to the satellite structure in the pulse spectra. Accordingly, the time–bandwidth product does not truly describe the pulse quality. In view of the deficiencies of the FWHM, a complementary concept using a root-mean-square (rms) width [7] was recently introduced to analyze the temporal and spectral features of ultra-short optical pulses. In this paper, we apply this rms formalism to characterize 10-fs pulses. We further demonstrate that the spectral and spatial control of laser pulses with an intracavity capillary and a slit in a Ti:sapphire laser resonator can substantially improve the spatial and spectral profiles of the pulses, reduce the rms width and hence improve the pulse quality.

*Corresponding author.
(Fax: +49-711/689-1615, E-mail: zhoujy@servix.mpi-stuttgart.mpg.de)

## 1 Theory

Ultra-short optical pulses can be well-described by the space–time Wigner distribution function (WDF) defined for the variables of spatial position $x$, spatial frequency $\xi$, time $t$ and frequency $\omega$ [9]. For a description of the spatial modes or the temporal behavior, the space-only or time-only WDF can be applied. Extensive research has been concerned with the characterization of the spatial beam quality using a space-only WDF description [10], and the beam quality has been characterized initially by the beam-waist radius and later by the spatial moment, in order to obtain a parameter which is applicable to complex shapes of the transverse-mode output and to partially coherent light beams where the beam radius is not very well defined [11]. The use of the spatial moment becomes indispensable when exploitation of the total gain volume of the laser medium is required for high-peak-intensity lasers. The generation of extremely short pulses reveals remarkable analogies to this situation in the spatial domain: the total bandwidth of the gain medium has to be utilized in order to achieve the necessary broadband emission. It is then an obvious idea to transfer the spatial moment formalism used for the characterization of the spatial beam quality to the time domain.

Theoretically, the optical field of a single transverse mode can be described by a WDF in the time–frequency domain [9]:

$$W^{\mathrm{T}}(\omega, t) = \frac{1}{N} \int E(t + t'/2)\, E^*(t - t'/2) \exp(-i\omega t')\, \mathrm{d}t' \,, \tag{1}$$

where $E$ is the electric field and $N$ is a normalization function. Let us define the temporal moment, $\langle \tau^2 \rangle$, by

$$\langle \tau^2 \rangle = \iint t^2 W^{\mathrm{T}}(\omega, t)\, \mathrm{d}t\, \mathrm{d}\omega = \int t^2 \left| E(t) \right|^2 \mathrm{d}t \,. \tag{2}$$

Comparison of (2) with the definition of the spatial moment, defined as $\langle x^2 \rangle = \int x^2 \left| E(x) \right|^2 \mathrm{d}x$, shows that the temporal

moment is described by exactly the same formalism. The rms width for optical pulses is defined as [8]

$$\tau_{\mathrm{rms}} = 2\sqrt{\langle\tau^2\rangle - \langle\tau\rangle^2} \tag{3}$$

with

$$\langle\tau^n\rangle = \frac{1}{N}\int_{-\infty}^{\infty} t^n I(t)\,\mathrm{d}t\,, \tag{4}$$

where $\langle\tau^2\rangle$ is the temporal moment and $N$ is a normalization constant given by $N = \int_{-\infty}^{\infty} I(t)\,\mathrm{d}t$.

The rms width can be experimentally determined from the intensity autocorrelation (AC) signal and is expressed as

$$\sigma^2 = \frac{1}{2N^2}\int_{-\infty}^{\infty} \tau^2 g(\tau)\,\mathrm{d}\tau\,, \tag{5}$$

where $N^2 = \int_{-\infty}^{\infty} g(\tau)\,\mathrm{d}\tau$, with $g(\tau) = \int_{-\infty}^{\infty} I(t+\tau)I(t)\,\mathrm{d}T$ being the intensity AC signal. Thus, the rms width can be obtained from $\tau_{\mathrm{rms}} = 2\sigma$. On the other hand, the rms width can also be directly determined from the interferometric autocorrelation (IAC). IAC ($s_2(\tau)$) and AC are related to each other by [12]

$$\begin{aligned} s_2(\tau) \propto 1 + 2g(\tau) + 4\mathrm{Re}\left[f_1(\tau)\exp(-i\omega_0\tau)\right] \\ + \mathrm{Re}\left[f_2(\tau)\exp(-2i\omega_0\tau)\right]\,, \end{aligned} \tag{6}$$

where

$$f_1 = \frac{1}{2}\int_{-\infty}^{\infty}\left[I(t) + I(t-\tau)E(t)E^*(t-\tau)\,\mathrm{d}t\right] \tag{7}$$

$$f_2 = \int_{-\infty}^{\infty} E^2(t)E^{*2}(t-\tau)\,\mathrm{d}t\,. \tag{8}$$

A figure of merit for chirp contamination of the pulses can be derived from AC or IAC traces:

$$C = \left[\left(\frac{\sigma}{\sigma_0}\right)^2 - 1\right]^{\frac{1}{2}} \tag{9}$$

with $\sigma_0$ the calculated temporal moment of the bandwidth-limited pulses, which can be derived either from the first-order autocorrelation or from the measured power spectrum through inverse Fourier transformation. The spectral moment is similarly defined as

$$\nu_{\mathrm{rms}} = 2\sqrt{\langle\nu^2\rangle - \langle\nu\rangle^2}\,. \tag{10}$$

The advantage of using the rms width is that no assumption concerning the pulse waveform is required and it can be evaluated directly from autocorrelation measurements. Furthermore, the rms width provides a more detailed measure of the pulses. Comparison of the FWHM width with the rms width for some characteristic pulse shapes was presented in [7]. It is obvious that optical pulses with a significant part of the energy in the pulse wings show a larger $\tau_{\mathrm{rms}}$ than pulses with a Fourier transform-limited time–bandwidth product. The prerequisite for obtaining the smallest possible $\tau_{\mathrm{rms}}$ is eliminating satellite pulses while maintaining a smooth and broad spectrum required for generation of pulses with a duration of a few cycles. This goal has been achieved in this work by utilizing intracavity spectral and spatial control.

## 2 Experimental

Our experiment is carried out with a home-built Ti:sapphire laser resonator with two quartz prisms and five mirrors, as shown in Fig. 1. The 4-mm-long Ti:sapphire laser crystal is pumped with the 5-W output of a frequency-doubled Nd:$YVO_4$ laser (Spectra Physics, Millenia). Four broadband high reflectors (HRs) and an output coupler with 3% transmission are employed in the resonator. One of the high reflectors is a chirped mirror [13], contributing to the intracavity dispersion compensation [4]. The residual chirp of the laser output is further compensated by a pair of external prisms and another chirped mirror. The output spectrum is recorded with an optical multichannel analyzer, and the temporal output is analyzed by taking first- and second-order autocorrelations using an actively stabilized Michelson interferometer [14]. It should be pointed out that the pulse spectrum can also be obtained by Fourier transforming the first-order autocorrelation trace.

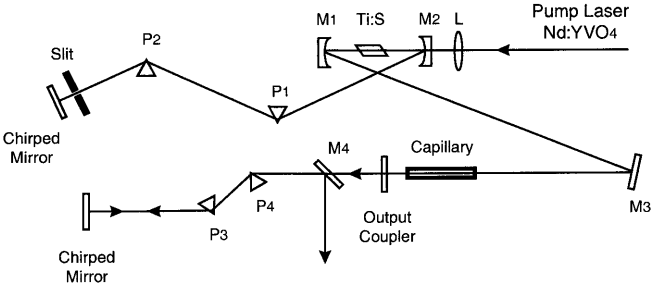


**Fig. 1.** Experimental arrangement of the Ti:sapphire laser oscillator producing high-quality 10-fs optical pulses

## 3 Results and discussion

For the Ti:sapphire laser resonator initially operating with an output coupler of 12% transmission, the output power goes up to 630 mW in continuous-wave mode, giving rise to a total power conversion of more than 12% with a pump power of 5 W. The output power is 550 mW when the laser is mode-locked and the laser spectrum and the beam cross section were smooth even without an intracavity aperture. In this situation, the pulse duration is longer than 20 fs, and the spectral bandwidth is less than 40 nm (FWHM), limited by the low intracavity intensity and the finite bandwidth of the output coupler. Alternatively, use of an output coupler with 3% transmission results in a mode-locked output power of 200 mW.

The laser was optimized with the 3% output coupler for spectrally broadband operation by controlling the insertion of

the quartz prisms into the laser beam. However, for spectral bandwidths exceeding 120 nm the laser output beam revealed significant divergence and spatially varying spectral structures. Figure 2a shows mode-locked laser spectra recorded through a horizontally placed slit shifted to different vertical positions of the laser beam cross section for a laser cavity without intracavity spatial and spectral control.

The measured spatial dependence of the pulse spectrum for broadband optical pulses was observed before and was referred to as the frequency-dependent mode size (FDMS) [5, 6]. For a fundamental Gaussian beam in a linear (intensity-independent), nondispersive laser cavity, the radius $w(z)$, as a function of propagation distance $z$, is given by [6]

$$w(z) = \sqrt{\frac{\lambda z_0}{\pi}} \left[ 1 + \left( \frac{z}{z_0} \right)^2 \right]^{\frac{1}{2}} \tag{11}$$

with $\lambda$ the wavelength and $z_0$ the confocal parameter. Since all the frequency components of the broadband radiation share the same confocal parameter in a laser resonator, the mode area is then proportional to the square root of the wavelength at position $z$, as determined by (11) for a passive cavity. Furthermore, (11) shows that the sub-structures in pulse spectra are related to the spatial structures for broadband laser output.

The real physical picture for an active cavity, however, is more complicated, since intensity-dependent nonlinear optical processes such as self-focusing and defocusing as well as self-phase modulation have to be taken into account. This suggests that a spatially resolved full characterization of the optical pulses is necessary, which can be fulfilled at present only with advanced spectral interferometry for direct electric-field reconstruction [6]. Otherwise, a spatially averaged measurement has to be used. A typical spatially averaged second-order autocorrelation and the corresponding spectrum for the complex-transverse-mode output from a laser cavity without any hard aperture are depicted in Figs. 3a and b, respectively. The second-order IAC (a) and the Fourier-transform spectrum (b) recorded for the Ti:sapphire oscillator without intracavity spectral and spatial mode control clearly reveal distinct modulation in the wings of the trace. The evaluated rms width is $\tau_{\mathrm{rms}} = 26.0$ fs and the spectral rms width is $\nu_{\mathrm{rms}} = 0.051 \times 10^{15}$ Hz, resulting in $\tau_{\mathrm{rms}} \nu_{\mathrm{rms}} = 1.39$.

High-quality optical pulses should have a single transverse mode so that the field can be described by a time-only WDF. Hence FWHM and rms widths can be unambigu-

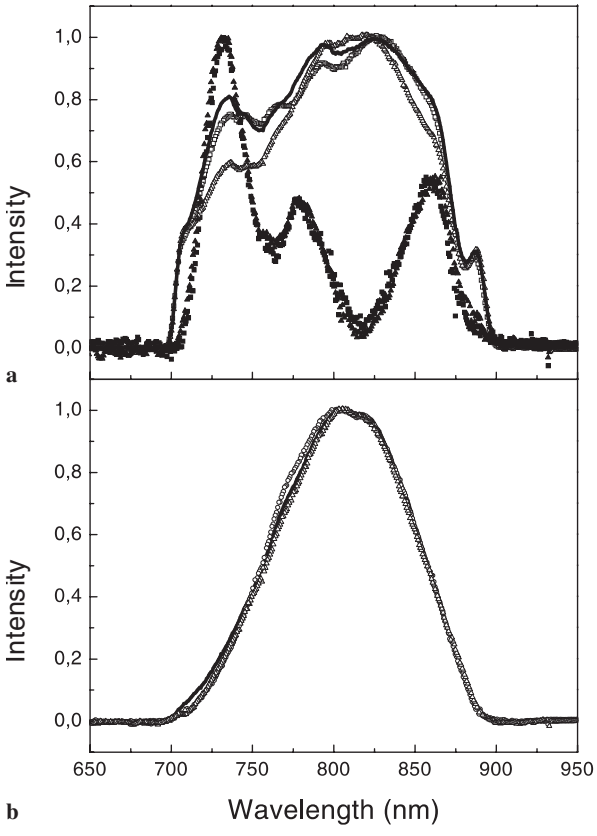


**Fig. 2. a** Spatially resolved spectra (normalized) measured for different vertical positions across the laser output beam from the oscillator without the slit and the capillary. The spot of the transverse mode is divided into four equal parts along the vertical direction. The spectra of the parts far from the spot center are represented by *filled squares* and *triangles* and the spectra of the parts near the spot center are shown by *open squares* and *triangles*. The averaged spectrum across the total beam profile is shown as a *solid line*. **b** Spatially resolved spectra for the lower parts (*open circles*), upper parts (*open triangles*) and the averaged spectrum (*solid line*) of the output for the laser with an intracavity capillary

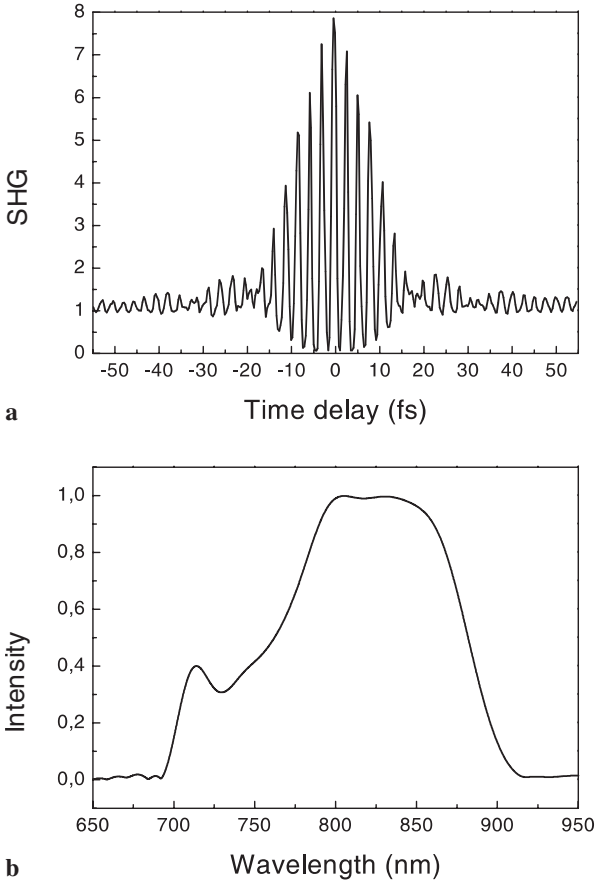


**Fig. 3a,b.** Second-order IAC (**a**) and the spectrum obtained by Fourier transforming the first-order autocorrelation (**b**) for the Ti:sapphire oscillator without intracavity spectral and spatial mode control. FWHM is $\tau_{\mathrm{FWHM}} = 15.5$ fs and $\tau_{\mathrm{rms}} = 26.0$ fs

ously determined from autocorrelation measurements. First, we tried to obtain single-transverse-mode operation of the broadband laser by inserting an intracavity hard aperture, but failed to suppress higher-order transverse modes unless the aperture diameter was reduced to less than 2 mm. The use of such a small-diameter aperture is necessary to provide sufficient mode discrimination defined as

$$\beta = \frac{\alpha_{01}}{\alpha_{00}}\,, \tag{12}$$

where $\alpha_{00}$ and $\alpha_{01}$ represent the resonator losses for the lowest- and the next higher-order transverse modes, respectively. Then a single transverse mode is achieved at the expense of low total output power of the laser. This also implies strong spectral filtering caused by the FDMS, and concomitantly the spectral bandwidth is strongly reduced [6].

It has been demonstrated previously that insertion of an intracavity capillary can substantially enhance the fundamental transverse mode power by simultaneously providing a small loss for the fundamental transverse mode and large mode discrimination, since an intracavity hollow waveguide leads to mode mixing among the free-space transverse modes and to energy transfer from complex transverse modes to a single transverse mode when it is properly placed inside the laser resonator. Insertion of an intracavity capillary can substantially enhance the mode discrimination and hence the fundamental transverse mode power [15]; namely, insertion of a waveguide results in a substantial improvement of the spatial mode pattern and the spectral profile. In our experiment, 8-cm-long capillaries with various inner-bore diameters have been inserted into the resonator. Those with diameters in the range of 2.5 mm to 3.0 mm have been found to be most suitable for generating optical pulses with smooth spatial and spectral profiles. Capillaries with larger diameter do not provide effective mode control, and those with smaller diameter limit the emission bandwidth and reduce the output power. With the optimum capillary (length 8 cm, internal diameter 2.6 mm) used in the experiment, nearly single transverse mode output with less than 20% loss of total power as compared to the case without any intracavity capillary has been obtained. The mode patterns of broadband laser output without and with an intracavity capillary are shown in Figs. 4a and b, respectively. The figures reveal substantial improvement of the transverse-mode pattern with the capillary. The single transverse mode output has a power of 160 mW. With intracavity spatial and spectral control, spatially resolved spectra for the lower (open circles) and upper (open triangles) parts of the laser output are shown in Fig. 2b. The averaged spectrum is depicted by the solid line.

Figure 5 shows the second-order autocorrelation trace and the corresponding spectrum for the resonator with an intracavity capillary (diameter 2.6 mm) and an adjustable slit. The FWHM of the autocorrelation trace is the same as that shown in Fig. 3. However, the root-mean-square width $\tau_{\mathrm{rms}} = 13.4$ fs is remarkably reduced in comparison to 26.0 fs shown in Fig. 3. The corresponding spectral rms width is $\nu_{\mathrm{rms}} = 0.042 \times 10^{15}$ Hz, which leads to $\tau_{\mathrm{rms}}\nu_{\mathrm{rms}} = 0.56$. The spectra shown in Fig. 5 are the measured spectrum (open circles) and the spectrum obtained by Fourier transforming the first-order autocorrelation (solid line), presenting a certain asymmetry. Good agreement is found for the measured pulse spectrum and the spectrum obtained by Fourier transform-

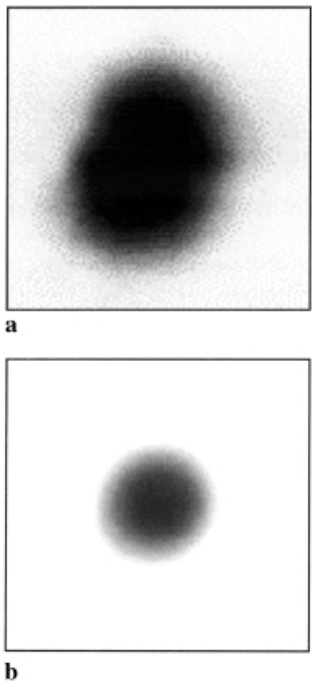


**Fig. 4a,b.** Mode pattern of the broadband laser output without (**a**) and with (**b**) an intracavity capillary

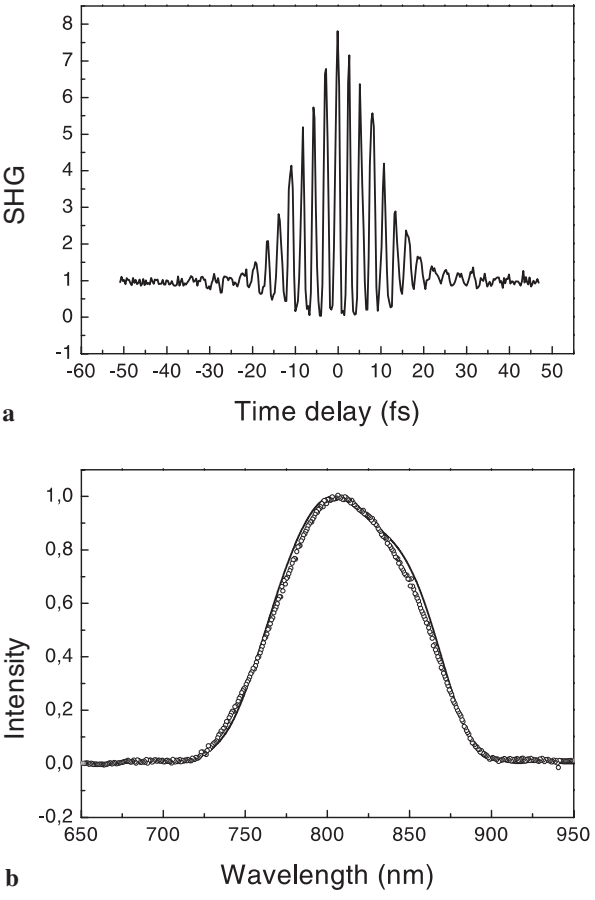


**Fig. 5a,b.** Second-order IAC (**a**), the corresponding measured spectrum (*open circles*) and the spectrum obtained by Fourier transforming the first-order autocorrelation (*solid line*) (**b**) for the Ti:sapphire oscillator with the intracavity capillary and an adjustable slit. FWHM is 15.5 fs and $\tau_{\mathrm{rms}} = 13.4$ fs

ation of the first-order autocorrelation, further demonstrating a homogeneous spectrum across the laser beam.

Figure 6 shows first- and second-order autocorrelations of laser pulses from a waveguide with a FWHM of 12 fs for Gaussian pulses with a spectral width $\nu_{\mathrm{FWHM}} = 47$ THz, leading to the time–bandwidth product $\tau_{\mathrm{FWHM}}\nu_{\mathrm{FWHM}} = 0.53$. In addition, $\tau_{\mathrm{rms}} = 13.0$ fs and $\nu_{\mathrm{rms}} = 0.046 \times 10^{15}$ Hz, resulting in $\tau_{\mathrm{rms}}\nu_{\mathrm{rms}} = 0.59$. In this case, the spectrally narrow satellite components appearing preferentially at the wings of the broadband spectrum have been completely eliminated by an adjustable vertical slit between prism $P_2$ and mirror $M_3$. Gaussian waveforms are applied simultaneously to fit the first- and second-order autocorrelations and the corresponding spectrum, which shows a spatially and temporally smooth, structureless profile. The spectrum corresponding to the pulse waveform presented in Fig. 6 is shown in Fig. 2b. The fitting to a Gaussian waveform rather than a sech waveform may be explained by intracavity spectral and spatial control, as the slit acts as a hard aperture and the waveguide acts as a soft aperture to reduce the spectral intensities in the wings of the broadband optical pulses. In addition, $C = 0.3$ indicates a good figure of merit for chirp contamination for the pulse shown in Fig. 5. On the other hand, numerical evaluation of the pulse shown in Fig. 3 gives rise to $C = 1.0$.

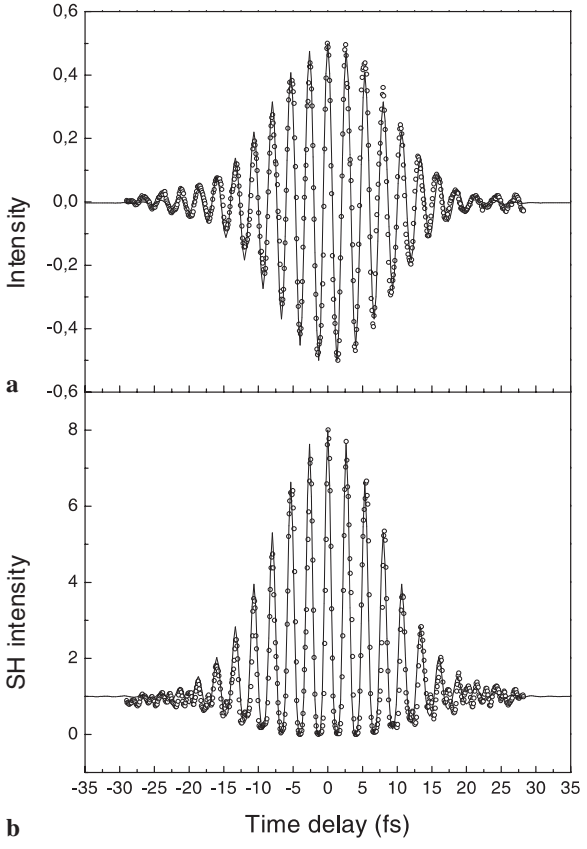


**Fig. 6a,b.** The first- and second-order autocorrelations of pulses with a FWHM of $\tau_{\mathrm{FWHM}} = 12$ fs and $\tau_{\mathrm{rms}} = 13$ fs. Experimental autocorrelations shown by open circles are fitted with Gaussian profiles (*solid lines* in (**a**) and (**b**)). The corresponding measured spectrum of the pulses is shown in Fig. 2b (*solid line*)

The residual small modulation appearing on the wings of the second-order autocorrelations (see Fig. 5a and Fig. 6b) is most likely due to a nonlinear chirp of the optical pulses and it is much less pronounced than the modulation of pulses generated without intracavity transverse mode control (see Fig. 3). The optical pulses are spectrally and temporally smooth with a nearly single transverse mode in the spatial domain. Such pulses are ideal for pulse amplification [16], for studies of pulse propagation [17] as well as for ultrafast spectroscopic investigations, especially those concerned with time-resolved phase spectroscopy [18] and phase control [19].

## 4 Conclusions

In conclusion, the quality of 10-fs optical pulses has been characterized using a root-mean-square formalism. By inserting an intracavity capillary and a slit in the laser cavity, efficient single transverse mode power and smooth spectral and temporal waveforms have been obtained.

*Acknowledgements.* The authors acknowledge K. Schubert for his contribution to the set-up and operation of the phase-locked Michelson interferometer and S. Linden and J. Prineas for critical reading of the manuscript. J. Cheng at ZSU contributed to this work by calculating the WDF and the rms width and part of that work is supported by the National Key Basic Research Special Foundation (NKBRSF) under Grant No. G1999075200. We also appreciate Prof. W.Z. Lin and his group in ZSU for experimental advice on the sub-10-fs laser system.

## References

1. J.P. Zhou, G. Taft, C.P. Huang, M.M. Murnane, H.C. Kapteyn, I.V. Christov: Opt. Lett. **19**, 1149 (1994)
2. L. Gallmann, D.H. Sutter, N. Matuschek, G. Steinmeyer, U. Keller, C. Iaconis, I.A. Walmsley: Opt. Lett. **24**, 1314 (1999)
3. L. Xu, G. Tempea, A. Poppe, M. Lenzner, Ch. Spielmann, F. Krausz, A. Stingl, K. Ferencz: Appl. Phys. B **65**, 151 (1997)
4. D.H. Sutter, L. Gallmann, N. Matuschek, F. Morier-Genoud, V. Scheuer, G. Angelow, T. Tschudi, G. Steinmeyer, U. Keller: Appl. Phys. B **70** (Suppl.), 5 (2000)
5. S.T. Cundiff, W.H. Knox, E.P. Ippen, H.A. Haus: Opt. Lett. **21**, 662 (1996)
6. L. Gallmann, G. Steinmeyer, D.H. Sutter, T. Rupp, C. Iaconis, I.A. Walmsley, U. Keller: Opt. Lett. **26**, 96 (2001)
7. E. Sorokin, G. Tempea, T. Brabec: J. Opt. Soc. Am. B **17**, 146 (2000)
8. B.C. Walker, C. Toth, D. Fittinghoff, T. Guo: J. Opt. Soc. Am. B **16**, 1292 (1999)
9. J. Paye, A. Migus: J. Opt. Soc. Am. **12**, 1480 (1995)
10. M.J. Bastiaans: J. Opt. Soc. Am. A **3**, 1227 (1986)
11. R. Martinez-Herrero, P.M. Mejias, N. Hodgson, H. Weber: IEEE J. Quantum Electron. **QE-31**, 2173 (1995)
12. K. Naganuma, K. Mogi, H. Yamada: IEEE J. Quantum Electron. **QE-25**, 1225 (1989)
13. K. Ferencz, R. Szipocs: Opt. Eng. **32**, 2525 (1993)
14. M.U. Wehner, M.H. Ulm, M. Wegener: Opt. Lett. **22**, 1455 (1997)
15. J.Y. Zhou, D.J. Zhou, Z.Z. Huang, Z.X. Yu: Opt. Commun. **74**, 75 (1989); J.Y. Zhou, C.H. Fu, Z.G. Lu, Q.X. Li, Z.X. Yu: Opt. Commun. **81**, 385 (1990)
16. S. Ranc, G. Cheriaux, S. Ferre, J.-P. Rousseau, J.-P. Chambaret: Appl. Phys. B **70** (Suppl.), 181 (2000)
17. H. Giessen, A. Knorr, S. Haas, S.W. Koch, S. Linden, J. Kuhl, M. Hetterich, M. Grün, C. Klingshirn: Phys. Rev. Lett. **81**, 4260 (1998)
18. Q. Luo, D.C. Dai, G.Q. Wang, V. Ninulescu, X.Y. Yu, L. Luo, J.Y. Zhou, Y.J. Yan: J. Chem. Phys. **114**, 1870 (2001)
19. M.U. Wehner, M.H. Ulm, D.S. Chemla, M. Wegener: Phys. Rev. Lett. **80**, 1992 (1998)